Atmos. Meas. Tech. Discuss., 3, 147–184, 2010
www.atmos-meas-tech-discuss.net/3/147/2010/

Atmospheric Measurement Techniques Discussions

This discussion paper is/has been under review for the journal Atmospheric Measurement Techniques (AMT). Please refer to the corresponding final paper in AMT if available.

The impact of surface reflectance variability on total column differential absorption LiDAR measurements of atmospheric CO_2

J. P. Lawrence[1], **R. J. Leigh**[1], **and P. S. Monks**[2]

[1]EOS Group, Department of Physics and Astronomy, University of Leicester, Leicester, LE1 7RH, UK
[2]EOS Group, Department of Chemistry, University of Leicester, Leicester, LE1 7RH, UK

Received: 28 September 2009 – Accepted: 23 December 2009 – Published: 11 January 2010

Correspondence to: P. S. Monks (p.s.monks@le.ac.uk)

Published by Copernicus Publications on behalf of the European Geosciences Union.

Abstract

The remote sensing technique, total column differential absorption LiDAR (TC-DIAL) has been proposed in a number of feasibility studies as a suitable method for making total column measurements of atmospheric CO_2 from space. Among the sources of error associated with TC-DIAL retrievals from space is an undefined modulation of the received signals resulting from the variability in the Earth's surface reflectance between the LiDAR pulses. This source of uncertainty is investigated from a satellite perspective by the application of a computer model for spaceborne TC-DIAL instruments. The simulations are carried out over Europe and South America using modified MODIS surface reflectance maps and a DIAL configuration similar to that suggested for the proposed ESA A-SCOPE mission. A positive bias of 0.01 ppmv in both continental test sets is observed using 10 Hz pulse repetition frequency and 200 km integration distance. This bias is a consequence of non-linearity in the DIAL equation, and in particular regions such as the Alps and over certain coastlines it contributes to positive errors of between 0.05 and 0.16 ppmv for 200 and 50 km integration distances. These retrieval errors are defined as lower bound estimates owing to the likely resolution difference between the surface reflectance data and the expected surface heterogeneity observed by a DIAL instrument.

1 Introduction

Carbon dioxide (CO_2) is a naturally and anthropogenically occurring green house gas in the Earth's atmosphere whose concentration has increased over the last 200 years by approximately 30% (Keeling et al., 1995). Measurements obtained from ice cores provide an historical account of atmospheric CO_2 concentrations as far back as 650 000 years, and via comparison with modern in-situ measurements it has been shown that the atmospheric CO_2 concentration is now over 90 ppmv higher then it has ever been in that time (Sitenthaler et al., 2005). The recent and sudden growth ob-

AMTD

3, 147–184, 2010

served has been attributed to anthropogenic activities such as the burning of fossil fuels, cement production and land-use change (IPCC, 2007).

Predicting the effect of increased CO_2 levels on the climate requires improved understanding of the terrestrial processes that control carbon fluxes, as well as any potential feedback mechanisms on these processes which may develop as a consequence of climate change (Sarmiento and Gruber, 2002). Tighter constraints on the transport models which at present are only capable of calculating fluxes on continental scales are required (Gibert et al., 2004). To better constrain the present models more observations are needed on a global scale to supplement the sparsely located in-situ measurement networks. Satellite remote sensing has been shown to provide the denser sampling required by inversion modeling and an improvement in flux estimation may be achieved if the precision of total column measurements averaged over monthly time scales on an $8^\circ \times 10^\circ$ footprint is less than 2.5 ppmv (Rayner and O'Brien, 2001). There are a number of satellite instruments at present measuring CO_2 from space including the SCIAMACHY instrument on board the ESA ENVISAT satellite (Bovensmann et al., 1999), the AIRS instrument onboard the NASA AQUA satellite, the IASI instrument onboard the METOP-A satellite and the GOSAT instrument launched by JAXA in January 2009 (Hamazaki et al., 2005). Whilst some of these systems may have shown the potential to meet the required spatial coverage and precision to improve flux estimates on continental scales (Barkley et al., 2006; Buchwitz et al., 2006), they also have limitations. In particular passive measurements which use the short wave infrared are limited by their reliance on solar illumination which restricts their latitudinal coverage, and thermal infrared systems are not sufficiently sensitive near the ground where the fluxes occur. Furthermore, passive remote sensing systems involve retrieval complexities which suffer from aerosol contamination and radiation path length uncertainties. The active remote sensing technique, total column differential absorption LiDAR (TC-DIAL) offers a different technique without some of these sources of uncertainty and has recently been the focus of many papers and feasibility studies (Amediek et al., 2009; Dufour and Breon, 2003; Ehret et al., 2008; Ehret and Kiemle, 2005; Gibert et al., 2004; Loth et al., 2005; Ismail et al., 2004). Many of TC-DIALs advantages over current passive remote sensing systems are a product of its use of pulsed (active) radiation. The path length of the returned pulses may be determined via the time between their transmission and reception, measurements can be made equally well at all latitudes both day and night, and by using a differential retrieval method, aerosol and thin cloud interference is avoided. These advantages make TC-DIAL a flexible CO_2 measuring technique capable of diurnal sampling with potential for near-surface sensitivity and therefore an attractive supplement to the current measurement systems (Loth et al., 2005). At present there are no CO_2 TC-DIAL instruments in space, however breadboard demonstrators and aircraft campaigns are being carried out to develop the technology for space application (Amediek et al., 2009).

The principle of TC-DIAL is the differential retrieval of scattered intensities from two laser transmissions of similar wavelengths. The wavelength of the first transmission is selected to be absorbed by CO_2 during its propagation through the atmosphere known as the "on-line" frequency, and the second transmission is tuned to avoid signficant absorption by CO_2 known as the "off-line" frequency (Fig. 1).

Two spectral lines have been identified as particularly appropriate for CO_2 DIAL using temperature sensitivity, strength and interference from other atmospheric species as selection criteria (Loth et al., 2005). The two lines identified were 4875.748957 and 6367.223459 cm^{-1}. The signal returned to the detector with which a CO_2 measurement is made is reflected from aerosols, cloud and the Earth's surface. For TC-DIAL only the latter applies by definition, however instruments which operate by this principle may also be able to use backscatter from clouds to retrieve above cloud CO_2 if the clouds are optically thick. The measurement pair consisting of the on-line and off-line returned intensities is used in a simple retrieval equation to calculate the vertical column density (VCD) of CO_2 in units of molecules per cm^2 (Eq. 1). The concentration is subsequently converted into a volume mixing ratio (VMR) (Ehret et al., 2008) (Eqs. 2 to 4).

$$n = \frac{1}{2\Delta\sigma(R_s - R_{toa})} \ln\left[\frac{S_{on}(R_{toa})S_{off}(R_s)}{S_{on}(R_s)S_{off}(R_{toa})}\right], \tag{1}$$

where n is the total column concentration of CO_2, $\Delta\sigma$ is the difference in absorption cross sections at the on-line and off-line wavelengths, S_{on} is the on-line signal strength, S_{off} is the off-line signal strength, R_{toa} is the range to the top of the atmosphere and R_s is the range to the surface.

$$N_{CO_2} = \frac{\tau}{\int_{-\infty}^{\infty} v\, dl}, \text{where} \tag{2}$$

$$\tau = \frac{1}{2} \ln\left(\frac{S_{on}}{S_{off}}\right), \text{and} \tag{3}$$

$$v(l) = \left[\frac{P(l)}{kT(l)} \cdot \frac{1}{1+\rho_w(l)}\right](\sigma_{on}(l) - \sigma_{off}(l)), \tag{4}$$

and N_{CO_2} is the CO_2 VMR, S_{on} and S_{off} are the on and off line intensities, respectively, k is the Boltzmanns constant, T is the temperature, P is the pressure, ρ_w is the water vapour concentration, σ_{on} and σ_{off} are the absorption cross sections for the online and offline pulses, respectively and l is the altitude.

Among the sources of error in TC-DIAL retrievals is the uncertainty associated with the spatial variability in the reflectance properties of the Earth's surface. The two surface footprints from the on and off-line transmissions do not completely overlap, and any variability in the surface reflectance across the footprints results in an error which varies as a function of distance between the footprint centre's and the surface reflectance variability.

The causes of the imperfect footprint co-location are laser pointing jitter owing to unavoidable vibrations within the spacecraft, and a time delay between the transmissions of the pulses designed to avoid any ambiguity in the retrieval owing to the simultaneous presence of the pulses in the atmosphere.

This paper investigates the regional, low bound errors incurred by the surface reflectance variability on TC-DIAL retrievals over Europe and South America. The study is carried out using a LiDAR model configured with the instrument and satellite specifications given in Table 1.

2 Methodology

The Leicester LiDAR model (LLM) simulates the physical processes associated with pulsed TC-DIAL systems, including interactions with clouds, aerosols, absorbing media and the Earth's surface. Its overall purpose is to investigate DIAL in its entirety and search for means of exploiting the technique in novel ways.

The model operates in one of three operational modes to suit the application. The single shot mode is used to investigate single pulse interaction with the surface and atmosphere, the batch mode is used to compare instrument and environmental properties, and the orbit mode simulates a TC-DIAL system using surface reflectance maps and orbit parameters to obtain retrievals as observed from a spaceborne platform.

2.1 Model atmosphere

The atmosphere model consists of a scattering component and an absorption component. The scattering component uses the Henyey-Greenstein approximation for the Mie phase function (Platt, 2008), a method required by scattering theory for the short wave infrared region of the electromagnetic spectrum (Eq. 5). The parameters which define the phase functions were obtained from the SCIATRAN database to allow the LLM to simulate various aerosol scenarios (Rozanov et al., 2002).

$$\Phi = \frac{1-g^2}{4\pi\left(1+g^2-2g\cos\theta\right)^{3/2}}, \tag{5}$$

where Φ is the phase function which describes the proportion of scattered photons in any direction within the plane of incidence, θ is the scattering angle and g is the asymmetry parameter.

The absorption component is based on a modified inversion of the Beer-Lambert equation (Eq. 6).

$$A = e^{-\Delta\sigma/n}, \tag{6}$$

where A is the fraction of light absorbed within the atmospheric level, l is the length of the atmospheric level, $\Delta\sigma$ is the absorption cross section difference between the on-line and off-line wavelengths and n is the concentration of CO_2 from the atmospheric CO_2 profile.

2.2 Model surface

The surface interaction is modelled using a bi-directional reflectance distribution function (BRDF) which is modified to account for the hot spot effect and DIAL viewing geometry (Eq. 7). The parameterisation for the function comes from the 500 m resolution MODIS BRDF data product MCD43A1.5 (Strahler et al., 1999), which for the present study required a culmination of three data sets for cloud clearing purposes. The dates used were the 5, 15 and 25 May 2007. The MODIS MCD43 product has been shown to have an RMS error of 0.0130 (equivalent to <5%) from continuous field observations of surface albedo at a number of measurement locations (Salomon et al., 2006).

$$R(\theta,\psi,\phi,\Lambda) = f_{\mathrm{iso}}(\Lambda) + f_{\mathrm{vol}}(\Lambda)K_{\mathrm{vol}}(\theta,\psi,\phi) + f_{\mathrm{geo}}(\Lambda)K_{\mathrm{geo}}(\theta,\psi,\phi) \tag{7}$$

The BRDF model used is a sum of three parameters (Roujean et al., 1992), f_{iso}, f_{vol} and f_{geo}, which combine to give surface reflectivity R. Two of the parameters have associated kernels, the volumetric kernel K_{vol} and the geometric kernel K_{geo} which provide the BRDF's directional components (Wanner et al., 1995).

The volumetric kernel (Eq. 8) is modified to account for the hot-spot effect (Maignan et al., 2003), a characteristic of nadir viewing LiDAR observations and anologous to viewing at the glint angle when observing the ocean with passive observations (Eq. 10).

$$K_{\mathrm{vol}} = \frac{4}{3\pi}\left[\frac{1}{\cos\theta_{\mathrm{s}} + \cos\theta_{\mathrm{v}}}\right]\cdot\left[F_{\mathrm{hs}}\left(\left(\frac{\pi}{2} - \xi\right)\cos\xi + \sin\xi\right)\right] - \frac{1}{3}, \tag{8}$$

where,

$$\cos\xi = \cos\theta_{\mathrm{s}}\cos\theta_{\mathrm{v}} + \sin\theta_{\mathrm{s}}\sin\theta_{\mathrm{v}}\cos\phi, \tag{9}$$

$$F_{hs} = \left(1 + \frac{1}{1+\xi/0.03}\right), \tag{10}$$

θ_s is the illumination azimuth angle, θ_v is the viewing azimuth angle, and ϕ is the illumination zentih angle.

The geometric kernel is given as

$$K_{geo} = O(\theta,\psi,\phi) - \sec\theta' - \sec\psi' + \frac{1}{2}(1+\cos\xi)(\sec\theta' \sec\psi'), \tag{11}$$

where,

$$O = \frac{1}{\pi}(t - \sin t \cos t)(\sec\theta' + \sec\psi'), \tag{12}$$

$$\cos t = \frac{1}{\pi}\frac{\sqrt{D^2 + (\tan\theta' \tan\psi' \sin\phi)^2}}{\sec\theta' + \sec\phi'}, \tag{13}$$

$$D = \sqrt{\tan^2\theta' + \tan^2\psi' - 2\tan\theta' \tan\psi' \cos\phi}, \tag{14}$$

$$\theta' = \tan^{-1}(\tan\theta), \tag{15}$$

$$\psi' = \tan^{-1}(\tan\psi). \tag{16}$$

The result of applying the BRDF model is a surface reflectance map (Figs. 2 and 3) in units of sr^{-1}.

An exception to the use of the BRDF calculations is the determination of the surface reflectance of water. In this instance it is assumed that the surface reflectance is $0.025\,sr^{-1}$ (Loth et al., 2005) and that the surface reflectance varies spatially with the same distribution function observed in the variation of available MODIS 1.6 µm water reflectance data. The figure chosen is the median of a reflectance distribution obtained from POLDER data for high sun elevation angles.

AMTD
3, 147–184, 2010

The pulse interaction with the surface is calculated using Eqs. (17) and (18) which define the scattered intensity of light from the surface back towards the detector. The on-line returned intensity (S_{on}) is the product of the surface reflectivity and the solid angle between the surface pixel and the satellite receiving mirror. The off-line returned intensity (S_{off}) is a sum of the on-line returned intensity and the difference between the on and off-line returned intensities taking account of the footprint overlap fraction labelled O in Fig. 4. The (S_{off}) term therefore may be considered to be the effective off-line intensity for the subsequent surface pixel having taken into consideration the footprint overlap.

$$S_{on} = \frac{R_{on}D}{L^2}, \tag{17}$$

$$S_{off} = S_{on} + \left(\frac{(R_{on} - R_{off})O \cdot D}{2L^2}\right), \tag{18}$$

where D is the receiver aperture diameter, O is the fractional area of the two footprints that do not overlap, R_{on} is the surface reflectance of the on-line footprint, R_{off} is the surface reflectance of the off-line footprint and L is the distance between the transmitter aperture and the ground. The values of D, O and L used in the model simulations are given in Table 1.

The resolution of the MCD43 product imposes limitations on the constraints which can be determined on errors incurred by surface reflectance variation. Variations in reflectance are expected to be observed over less than 50 m, yet the MODIS data product provides an average figure over 500 m. On the scale of individual pulses, the lower resolution of the MODIS datasets will reduce variations owing to smaller scale objects, however the integration distance of the DIAL instrument will aid in reducing the statistical impact of this effect. Despite this consolidation it must be accepted that the variations observed in this study are somewhat lower than those a DIAL system will encounter, and by consideration of this the aim of this study is to assess regional variations in the errors incurred in the DIAL retrievals, and to determine lower bound errors for those variations.

2.3 Model spectroscopy

The LLM incorporates spectral line shape calculations founded on HITRAN 2008 line centers and associated parameters to define the position and behavior of the relevant spectral lines (Lafferty et al., 2009). A convolution algorithm constrained by these parameters is applied to the lines with a pressure and temperature dependant Voigt line shape (Mitchell, 1971). The result of the convolution process is a vertically varying group of spectral lines, incorporating collisional and pressure broadening as well as pressure shift (Eq. 19).

$$V(x) = \frac{\alpha \upsilon_0}{\pi\left(\sqrt{\pi}\gamma_D\right)} \int_{-\infty}^{\infty} \frac{e^{-t^2/\gamma_D^2}}{(v-t)^2+\alpha^2} dt, \tag{19}$$

where

$$\gamma_D = \Delta_D \sqrt{\ln 2}, \tag{20}$$

$$\alpha = \sqrt{\ln 2}\left(\frac{\Delta_L}{\Delta_D}\right), \tag{21}$$

$$\Delta_D = \left(\frac{\Delta_L}{\pi}\right)\left(\frac{1}{(\upsilon-\upsilon_0)^2+\Delta_L}\right), \tag{22}$$

$$\Delta_L = \mathrm{Ref}\left(\frac{P}{101325}\right)\left(\frac{273}{T}\right)^{1/2}. \tag{23}$$

Ref is the spectral lines half width at half maximum at a reference atmospheric temperature and pressure. For HITRAN, and therefore the LLM, these points are 101 325 Pa and 273 K. υ is the wavenumber of the laser transmission, υ_0 is the centre lines wave

AMTD

3, 147–184, 2010

DIAL measurement bias owing to surface reflectance variability

J. P. Lawrence et al.

number (4875.74896 cm^{-1}), P is the atmospheric pressure and T is the atmospheric temperature. The atmospheric profiles used with the Voigt lineshape calculations are MIPAS reference atmospheres (Remedios et al., 2007).

Three spectral lines were chosen to be modelled based on their proximity to the on-line laser frequency and their absorption cross sections. The omission of the other spectral lines was investigated and resulted in a retrieval difference of approximately 4.0×10^{-4} ppmv.

In Fig. 5 the spectral line strengths are displayed as a function of distance from the primary line centre (4875.74896 cm^{-1}), with 9 spectral lines identified as most important based on their strength and proximity to the centre line.

2.4 Error estimation

For DIAL measurements to meet precision requirements they must be averaged over an interval of time. The size of this interval depends on the desired spatial resolution and the instrument pulse repetition frequency (PRF). To combine the uncertainties normal distribution statistics may be applied if the associated errors are approximately Gaussian in shape and non-biased. Analysis of the errors incurred in the CO_2 retrievals by the variability in the surface reflectance over Europe is given in Fig. 6.

A non-skewed Gaussian distribution of amplitude 45 900.0 and standard deviation 1.05 is fitted to the histogram using a least squares fitting method. Given the reasonable fit observed the use of Gaussian error statistics is viable, and Eq. (24) is used to combine the individual errors in the present study.

$$Z = \frac{\sum_0^n (z_i)}{n\sqrt{n}}, \tag{24}$$

where Z is cumulative error over the integration distance, n is the number of measurements and z is the error associated with each individual measurement.

2.5 Model configuration

The LiDAR model is configured using parameters partly based on the expected configuration of the A-SCOPE mission (A-SCOPE, 2008) and these are presented in Table 1. Using these parameters the model operates with an optimum precision of $\pm 2.0 \times 10^{-5}$ ppmv when no sources of error are applied. The locations chosen for the investigation are Europe and South America. Europe was identified as an ideal location to observe errors associated with measurements intersecting coastlines owing to its variety of land mass shapes, and South America was chosen because of its importance as a carbon sink.

The error associated with surface reflectance variability for a single sounding varies as a function of footprint overlap and the surface's reflectance heterogeneity over the area of the footprints (Fig. 7).

The separation between the footprint centres is a fixed value for the simulations performed as per Table 1, and the surface reflectance variability is dependant on the geolocation of the measurements. However, for multiple soundings integrated over an interval in time, the pulse repetition frequency and the integration interval are variables which also affect the errors observed. The retrieval error response to varying the PRF and the integration interval is investigated for 50, 100 and 200 km integration distances and for 1 to 10 Hz PRF. The limits on the variables are based on the restrictions imposed by the resolution of the surface reflectance map. For 10 Hz the measurement pairs are approximately 700 m apart and therefore approaching the limit of the model resolution at 500 m, and at 1 Hz the measurement pairs are approximately 7 km apart allowing only 7 measurements to be integrated within 50 km.

3 Results

The results from both continental test patches show variability in the surface reflectance which leads to biases in the TC-DIAL retrievals. They also show that particular geographic features such as mountain regions and coastlines create errors which significantly exceed the average. These features and their relationships to associated variables are described here.

3.1 Bias

The presence of a bias in the retrieval is a consequence of non-linearity in the DIAL equation and has been shown to be of similar magnitude over both Europe and South America. A recent aircraft campaign looking at the effect of surface reflectance variability on DIAL retrievals used a power series expansion to the first order to linearise the DIAL equation with the effect of successfully avoiding a bias in their result sets (Amediek et al., 2009). Unfortunately this method is only applicable to measurements where the on-line and off-line returned intensities are of similar strength. In conditions typical of a spaceborne system the returned intensities are likely to be significantly different rendering this approximation unsuitable for spaceborne retrievals.

The bias has been shown to vary with both integration distance and pulse repetition frequency. Simulated measurements over the Amazon rainforest are a suitable example of this with the bias ranging from 0.08 ppmv to 0.02 ppmv for variations of 1 to 10 Hz PRF and 50 to 200 km integration distance.

Comparing the results from the Amazon rainforest with that of the entire continental region shows that the magnitude of the bias is diluted by the presence of relatively homogeneous surfaces such as water. For all of South America the bias is approximately 0.01 ppmv lower on average than it is over the Amazon rainforest alone.

3.2 Regional errors

Figures 8 and 9 highlight particular regions where the measurement errors far exceed the average. These include the Alps, the west coast of Scotland, the mountains of Norway, the east coast of Sweden, the north west of the Andes mountain range and many other regions where the orbit track has been repeatedly intersected by coastlines.

Figures 10 and 11 show the simulation data over Europe and South America. The error spikes associated with mountains and coastlines are clearly identifiable as is a positive bias.

3.3 Integration distance

The integration distance determines the number of the measurements averaged over and may be increased to reduce measurement errors through statistical averaging at the expense of spatial resolution. Three data sets with integration distances of 50, 100 and 200 km are presented in Fig. 12.

To quantify the effect of integration distance, the mean bias and the top one percentile values are tabulated for the Europe and South America result sets in Tables 2 and 3, respectively. The top 1% errors were investigated as a seperate statistic for their strong association with mountain regions and coastlines and as a means to provide an indication as to the response of the errors over these regions to variations in instrument configuration.

The distribution of the errors over both continents are quantified by the least squares fitting of a skewed normal distribution function to the error histograms for 50, 100 and 200 km integration distances. The fits are given in Fig. 13 and the parameters of the skewed normal distribution fits are tabulated in Tables 4 and 5.

The function for the skewed normal distributions fitted to the histograms is given in Eq. (25) (Azzalini, 1985).

$$f(x) = \frac{2\alpha}{pb^2 2\pi} e^{-\left(\frac{(x-a)^2}{2b^2}\right)} \int_{-\infty}^{\alpha x} e^{-\left(\frac{(\alpha x - a)^2}{2b^2}\right)} dx, \tag{25}$$

where α is the skew factor, p is the amplitude factor which modifies the normalised amplitude, b is the standard deviation and a is the offset in the x domain.

AMTD

3, 147–184, 2010

3.4 Pulse repetition frequency

The pulse repetition frequency defines the number of measurements made within a given integration interval. The effect of changing the PRF on the measurement bias and top 1% errors are investigated and presented in Fig. 14 for 50, 100 and 200 km integration distances over key locations. The locations are the Alps and the west coast of Scotland to consider mountain and coastline regions, and the Amazon rainforest to include an example of a large area with a relatively homogenous surface.

The presented results show that increasing the PRF reduces the retrieval error for both the bias and the top 1% error components over very different error source locations, however, based on the trends observed in Fig. 14 very little improvement is expected after 10 Hz. The trends are likely to be a combination of a reduction in error with increased PRF as a result of greater statistical averaging, and an increase in error as a result greater exposure to potential surface variability.

The uncertainty in the presented results arises from the error in the variability of the surface reflectance between adjacent pixels, and therefore can be up to twice that of the uncertainty in the MODIS MCD43 product, implying an error of <10% for all results. A further source of error is the resolution difference between the MODIS pixel and the surface reflectance variations on the scale of the overlap of the two DIAL footprints. This ambiguity incurs an underestimation of the surface variability and as a consequence leads to an underestimation in the errors as well. It is accepted as a result that the magnitude of the errors observed are lower bound estimates.

4 Conclusions

The study has shown the lower bound errors incurred in DIAL retrievals as a consequence of the Earth's surface reflectance variability. A bias observed over both continental regions has been quantified over a range of instrument parameters within the limits of the LiDAR model capabilities, and the findings show that the bias magnitude is strongly dependant on the instrument pulse repetition frequency and the along-track integration distance. The cause of the bias has been concluded to be a result of uncertainties existing in the returned laser pulses intensities within the non-linear DIAL equation. The spatial component of the retrieval errors was also investigated and showed that mountain ranges and coastlines that repeatedly intersect the orbit track are the most detrimental features to the retrieval, and that the magnitude of these values are also dependent on the integration distance and instrument pulse repetition frequency.

From the findings of this study it may be inferred that any mountain region and coastline with comparable surface angle to the satellites surface track may result in an error that exceeds those quantified as top 1% errors in this study. It may be possible to compensate for this in the retrieval process if the expected biases were accurately quantified over these regions. This would would require the inclusion of seasonal variations in land type and cover, as well as potentially tides and receding coastlines. Further investigation using higher resolution reflectance data such as that from Landsat will aid in obtaining more accurate error estimates.

Acknowledgements. This work was funded under a studentship provided by the Centre for Earth Observation Instrumentation (CEOI), the authors would also like to thank Brian Perrett of QinetiQ for guidance and information towards realistic instrument parameterisation within the Leicester LiDAR model.

References

Amediek, A., Fix, A., Ehret, G., Caron, J., and Durand, Y.: Airborne lidar reflectance measurements at 1.57 µm in support of the A-SCOPE mission for atmospheric CO_2, Atmos. Meas. Tech., 2, 755–772, 2009, http://www.atmos-meas-tech.net/2/755/2009/. 149, 150, 159

Azzalini, A.: A class of distributions which includes the normal ones, Scand. J. Stat., 12, 171–178, 1985. 160

Barkley, M. P., Monks, P. S., Frieß, U., Mittermeier, R. L., Fast, H., Körner, S., and Heimann, M.: Comparisons between SCIAMACHY atmospheric CO_2 retrieved using (FSI) WFM-DOAS to ground based FTIR data and the TM3 chemistry transport model, Atmos. Chem. Phys., 6, 4483–4498, 2006, http://www.atmos-chem-phys.net/6/4483/2006/. 149

Burrows, J. P., Buchwitz, M., Frerick, J., Noël, S., Rozanov, V. V., Chance, K. V., and Goede, A. H. P.: SCIAMACHY – Mission objectives and measurement modes, J. Atmos. Sci., 56, (2), 127–150, 1999. 149

Buchwitz, M., de Beek, R., Noël, S., Burrows, J. P., Bovensmann, H., Schneising, O., Khlystova, I., Bruns, M., Bremer, H., Bergamaschi, P., Körner, S., and Heimann, M.: Atmospheric carbon gases retrieved from SCIAMACHY by WFM-DOAS: version 0.5 CO and CH_4 and impact of calibration improvements on CO_2 retrieval, Atmos. Chem. Phys., 6, 2727–2751, 2006, http://www.atmos-chem-phys.net/6/2727/2006/. 149

Dufour, E. and Breon, F.: Spaceborne estimates of atmospheric CO_2 column by use of the differential absorption method: error analysis, Appl. Optics, 42, 3595–3609, 2003. 149

Ehret, G., Kiemle, C., Wirth, M., Amediek, A., Fix, A., and Houweling, S.: Spaceborne remote sensing of CO_2, CH_4 and N_2O by integrated path differential absorption lidar: A sensitivity analysis, Appl. Phys. B-Lasers O., 90, 593–608, 2008. 149, 150

Ehret, G. and Kiemle, C.: Final rep. ESA study 10880/03/NL/FF, 2005. 149

European Space Agency (ESA): A-SCOPE 2013 advanced space carbon and climate observation of planet earth, report for assessment, ESA-SP1313/1, 2008. 158

Gilbert, F., Flamant, P. H., Bruneau, D., and Loth, C.: Heterodyne dial measurements of atmospheric CO_2 numerical simulation and experimental results, 22nd International Laser Radar Conference (ILRC 2004), in: Proceedings of the Conference held 12–16 July, 2004 in Matera, Italy, edited by: Pappalardo, G. and Amodeo, A., ESA SP-561, Paris: European Space Agency, 2004. 149

Gurney, K., Law, R. M., Denning, A. S., Rayner, P. J., Baker, D., Bousquet, P., Bruhwiler, L., Chen, Y., Ciais, P., Fan, S., Fung, I. Y., Gloor, M., Heimann, M., Higuchi, K., John, J., Maki, T., Maksyutov, S., Masarie, K., Peylin, P., Prather, M., Pak, B. C., Randerson, J., Sarmiento, J. L., Taguchi, S., Takahashi, T., and Yuen, C.: Towards robust regional estimates of CO_2 sources and sinks using atmospheric transport models, Nature, 415, 626–630, 2002.

Hamazaki, T., Kaneko, A., Kuze, A., and Kondo, K.: Fourier transform spectrometer for greenhouse gases observing satellite (GOSAT), Enabling sensor and platform technologies for spaceborne remote sensing, SPIE proceedings, 5659, 73–80, 2005. 149

IPCC: Climate change 2007 the physical science basis, contribution of Working Group 1 to the Fourth Assessment Report of the Intergovernmental Panel on Climate Change, Cambridge, 137–140, 996 pp.,2007. 149

Ismail, S., Koch, G. J., Barnes, B. W., Abedin, N., Refaat, T. F., Yu, J., Vay, S. A., Kooi, S., Browell, E., and Singh, U. N.: Technology developments for tropospheric profiling of CO_2 and ground-based measurements, 22nd International Laser Radar Conference (ILRC 2004), in: Proceedings of the Conference held 12–16 July, 2004 in Matera, Italy, edited by: Pappalardo, G. and Amodeo, A., ESA SP-561, Paris: European Space Agency, 65, 2004. 150

Keeling, C. D., Whorf, T. P., Wahlen, M., and Van der Plicht, J.: Interannual extremes in the rate of rise of atmoshperic carbon dioxide since 1980, Nature, 375, 666–670, 1995. 148

Lafferty, W., Mandin, J.-Y., Massie, S. T., Mikhailenko, S. N., Miller, C. E., Moazzen-Ahmadi, N., Naumenko, O. V., Nikitin, A. V., Orphal, J., Perevalov, V. I., Perrin, A., Predoi-Cross, A., Rinsland, C. P., Rotger, M., Simeckova, M., Smith, M. A. H., Sung, K., Tashkun, S. A., Tennyson, J., Toth, R. A., Vandaele, A. C., and Auwera, J. V.: The hitran 2008 molecular spectropscopic database, J. Quant. Spectrosc. Ra., 110, 533–572, 2009. 156

Loth, C., Flamant, P. H., Breon, F., Bruneau, D., Desmet, P., Pain, T., Dabas, A., Prunet, P., and Cariou, J.: The future of atmospheric carbon dioxide testing from space, ESA study 17852/04/NL/CB, IPSL, 2005. 150, 154

Maignan, F., Breon, F.-M., and Lacaze, R.: Bidirectional reflectance of earth targets: Evaluation of analytical models using a large set of spaceborne measurements with emphasis on the hot spot, Remote Sens. Environ., 90, 210–220, 2003. 153

Mitchell, A. G. G. and Zemansky, M. W.: Resonance Radiation and Excited Atoms, Cambridge University Press, 158–162, 338 pp., 1971. 156

Platt, U., Stutz, J., Guzzi, R., and Lanzerotti, L. J.: Differential Optical Absorption Spectroscopy: Principles and Applications, 99–102, Springer, 500 pp., 2008. 152

Rayner, P. J. and O'Brien, D. M.: The utility of remotely sensed CO_2 concentration data in surface source inversions, Geophys. Res. Lett., 28, 175–178, 2001. 149

Remedios, J. J., Leigh, R. J., Waterfall, A. M., Moore, D. P., Sembhi, H., Parkes, I., Greenhough, J., Chipperfield, M. P., and Hauglustaine, D.: MIPAS reference atmospheres and comparisons to V4.61/V4.62 MIPAS level 2 geophysical data sets, Atmos. Chem. Phys. Discuss., 7, 9973–10017, 2007, http://www.atmos-chem-phys-discuss.net/7/9973/2007/. 157

Roujean, J., L. M., Deschamps, P.: A bidirectional reflectance model of the earth's surface for

AMTD

3, 147–184, 2010

DIAL measurement bias owing to surface reflectance variability

J. P. Lawrence et al.

the correction of remote sensing data, Geophys. Res. Lett., 97, 20, 455–20, 468, 1992. 153
Rozanov, V. V., Buchwitz, M., Eichman, K. U., De Beek, R., and Burrows, J. P.: Sciatran – a new radiative transfer model for geophysical applications in the 240–2400 nm spectral region: the pseudo-spherical version, Adv. Space Res., 29, 1831–1835, 2002. 152
Salomon, J. G., Schaaf, C. B., Strahler, A. H., Gao, F., and Jin, Y.: Validation of the MODIS bidirectional reflectance distribution function and albedo retrievals using combined observations from the aqua and terra Platforms, IEEE T. Geosc. Remote, 44, 6, 1555–1565, 2006. 153
Sarmiento, J. L. and Gruber, N.: Sinks for anthropogenic carbon, Phys. Today, 30–36, 2002. 149
Siegenthaler, U., Stocker, T. F., Monnin, E., Luthi, D., Scheander, J., Stauffer, B., Ratynaud, D., Barnola, J., Fischer, H., Masson-Delmotte, V., and Jouzel, J.: Stable carbon cycle-climate relationship during the later pleistocene, Science, 310, 131–137, 2005. 148
Strahler, A. H., Muller, J.-P., Lucht, W., Schaaf, C. B., Tsang, T., Gao, F., Li, X., Lewis, P., and Barnsley, M. J.: MODIS BRDF/Albedo Product: Algorithm Theoretical Basis Document, 1999. 153
Wanner, W., Li, X. and Strahler, A. H.: On the derivation of kernels for kernel-driven models of bidirectional reflectance, Geophys. Res. Lett., 100, 21077–21089, 1995. 153

Table 1. List of model parameters used in the LLM for this study.

Model Parameter	Setting
Simulation duration	29 days
Atmospheric depth	60 km
Satellite altitude	400 km
Modelled spectral lines	3
Orbit inclination	82°
On/Off footprint seperation	12 m
Pulse repetition freq	10 Hz
Spectral line centre	$4875.74896\,\mathrm{cm}^{-1}$
On-line offset	$0.08\,\mathrm{cm}^{-1}$
Off-line offset	$0.7\,\mathrm{cm}^{-1}$
Transmission energy	0.1 J/pulse
Power distribution off/on	1/3
Laser line width	1 MHz
Laser pulse width	100 ns
Instrument sampling	500 ns
Receiver diameter	1 m
Quantum efficiency	61%
Optical efficiency	90%

AMTD
3, 147–184, 2010

Table 2. Mean errors and top 1% errors associated with various integration distances over Europe for 10 Hz simulated DIAL data.

Integration distance (km)	LLM error mean (ppmv)	Top 1% errors (ppmv)
50	0.0168	0.13
100	0.0121	0.07
200	0.0086	0.05
400	0.0061	0.02

Table 3. Mean errors and top 1% errors associated with various integration distances over South America for 10 Hz simulated DIAL data.

Integration distance (km)	LLM error mean (ppmv)	Top 1% errors (ppmv)
50	0.0204	0.16
100	0.0143	0.09
200	0.0102	0.06
400	0.0098	0.04

AMTD

3, 147–184, 2010

Title Page
Abstract Introduction
Conclusions References
Tables Figures
Back Close
Full Screen / Esc
Printer-friendly Version
Interactive Discussion

Table 4. Skewed normal distribution parameters used to fit retrieval histograms for various integration distances over Europe.

Integration distance	α	b	a	p
50	49.5	0.31	−0.28	2.21
100	91.8	0.25	−0.32	2.18
200	114.2	0.24	−0.33	2.31

Table 5. Skewed normal distribution parameters used to fit retrieval histograms for various integration distances over South America.

Integration distance	α	b	a	p
50	91.2	0.48	−0.62	0.95
100	117.0	0.38	−0.57	0.95
200	149.0	0.31	−0.51	0.95

AMTD
3, 147–184, 2010

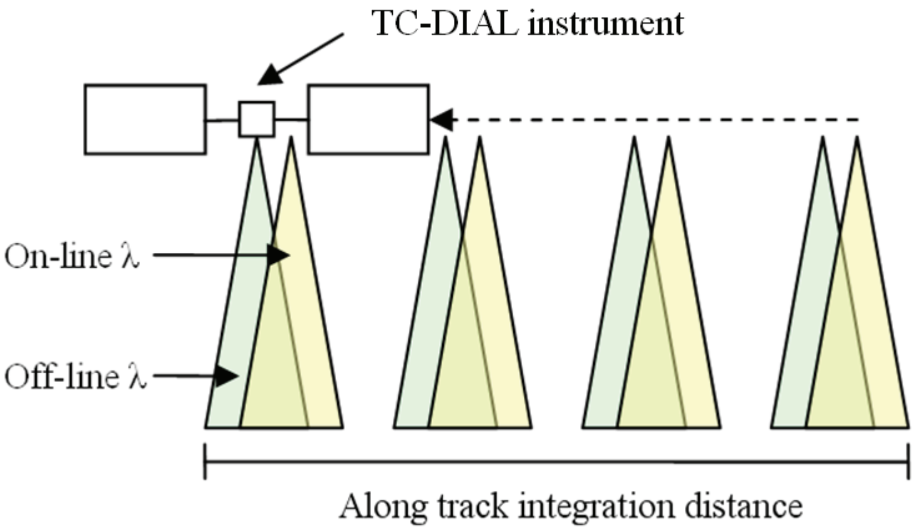

Fig. 1. Diagrammatic representation of the DIAL measurement process showing four soundings within an integration interval. The two transmissions which make up a single measurement are closely located but do not completely overlap.

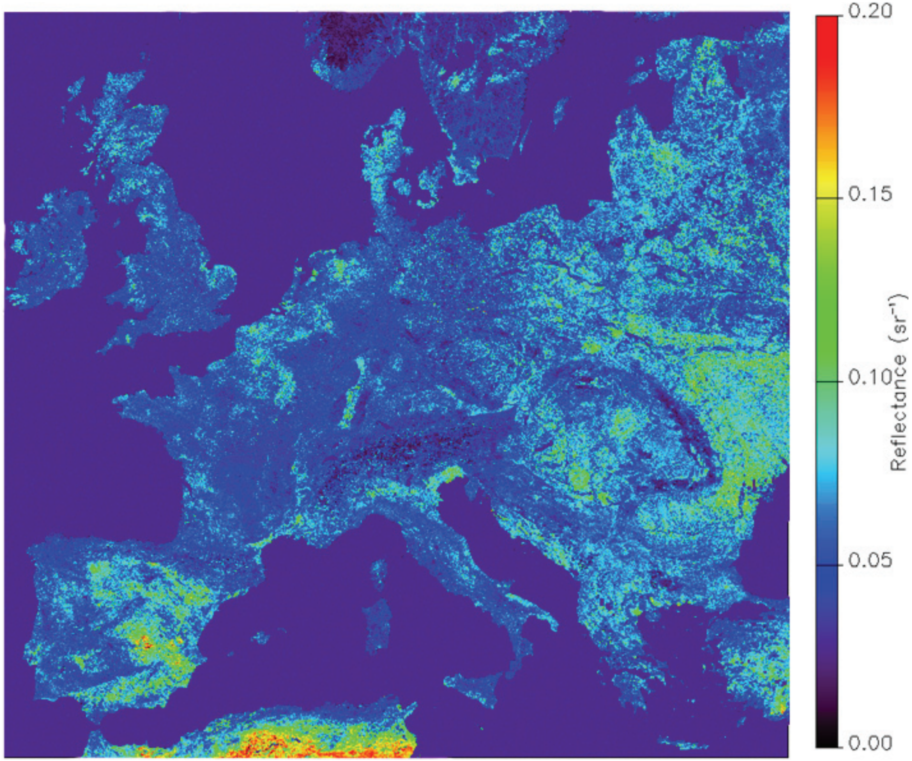

Fig. 2. Surface reflectance map over Europe generated by the Leicester LiDAR Model at 500 m resolution.

AMTD

3, 147–184, 2010

DIAL measurement bias owing to surface reflectance variability

J. P. Lawrence et al.

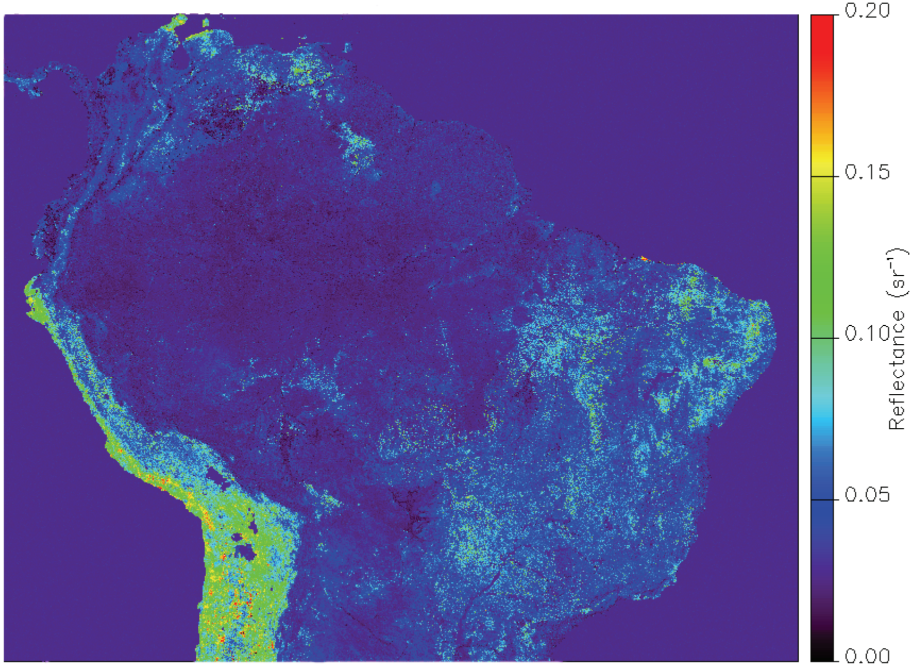

Fig. 3. Surface reflectance map over South America generated by the Leiceter LiDAR Model at 500 m resolution.

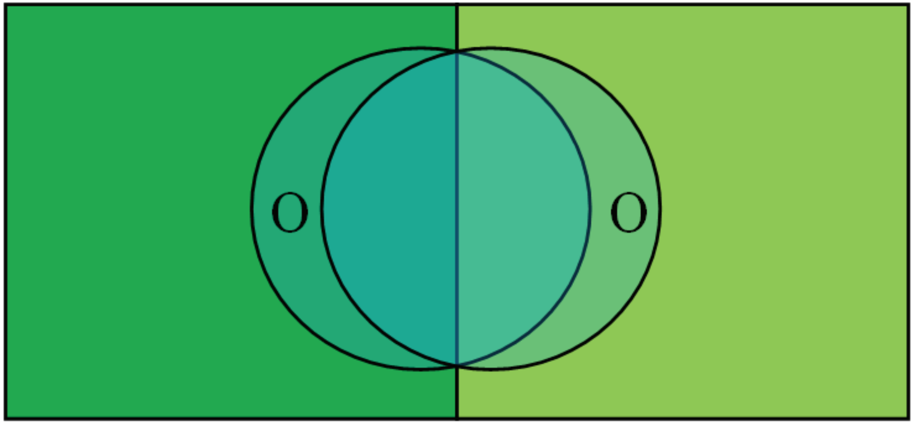

Fig. 4. A schematic representation of DIAL surface area viewing geometry over lower resolution MODIS pixels (not to scale).

AMTD
3, 147–184, 2010

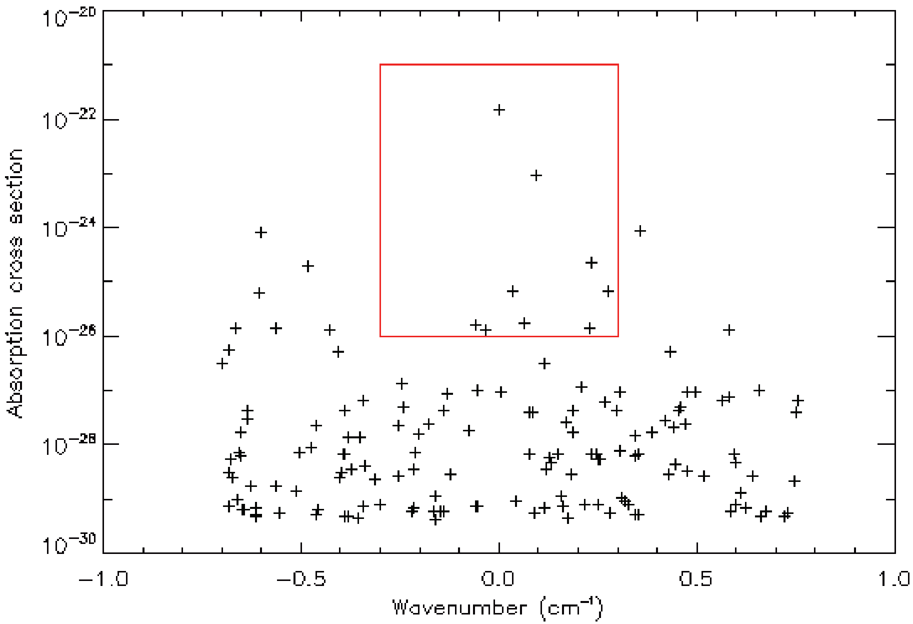

Fig. 5. HITRAN 2008 line centre positions and cross sections.

AMTD

3, 147–184, 2010

DIAL measurement bias owing to surface reflectance variability

J. P. Lawrence et al.

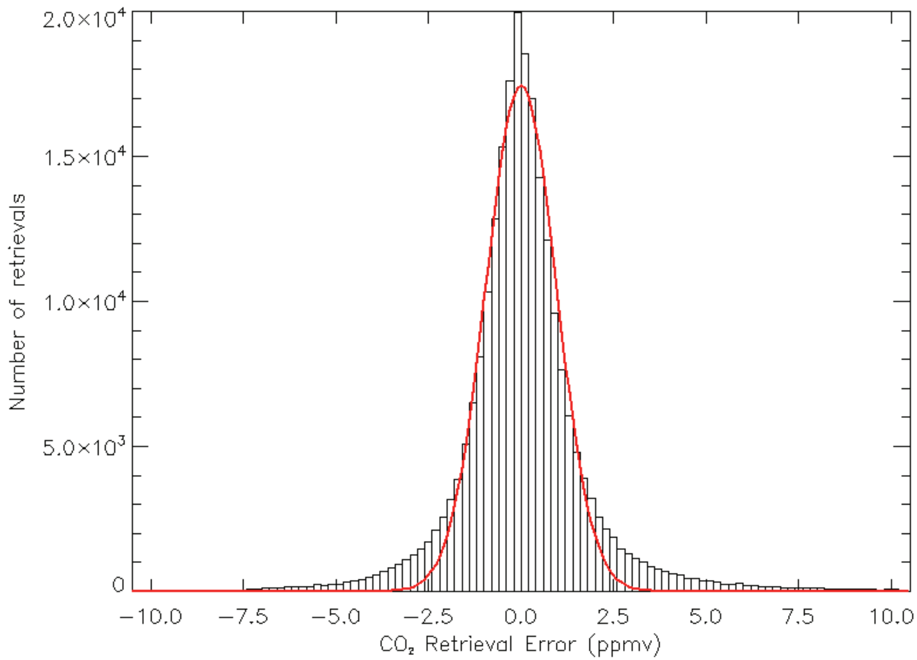

Fig. 6. Histrogram of CO_2 retrieval errors over Europe with fitted Gaussian distribution.

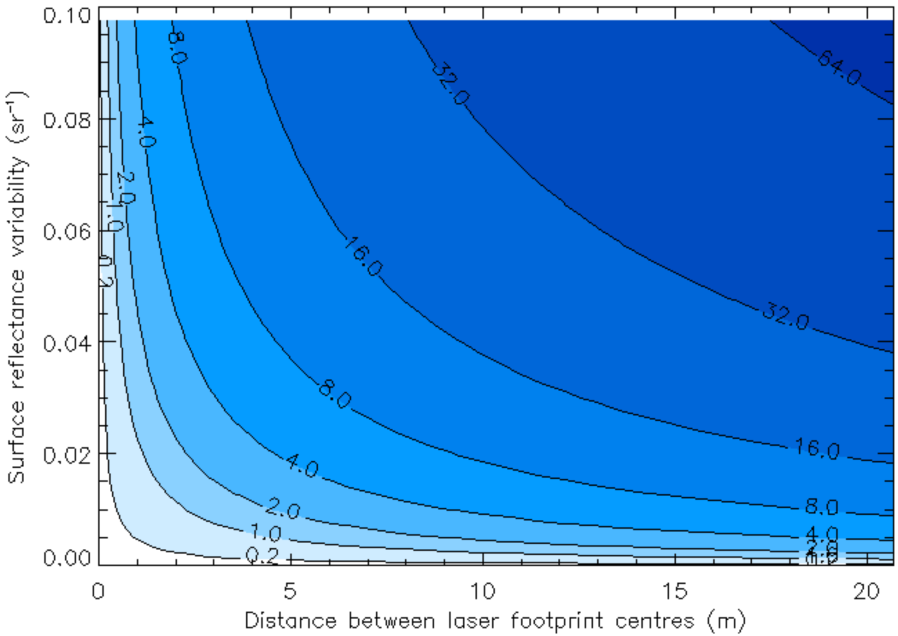

Fig. 7. CO_2 retrieval error (ppmv) as a function of surface reflectance variability and distance between footprint centres for a single sounding. Data generated by the Leicester LiDAR model using system parameters as per Table 1.

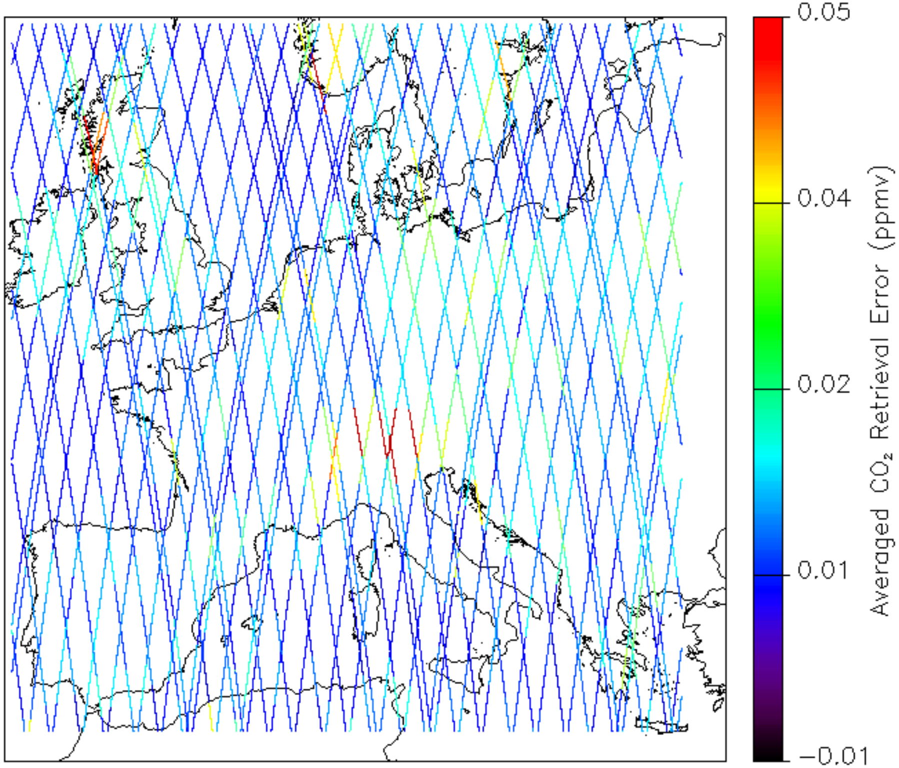

Fig. 8. CO_2 retrieval error in units of ppmv over Europe for one month of 10 Hz simulated DIAL data integrated over 200 km intervals. The scale has been truncated to 0.05 to allow for stronger contrasts.

AMTD

3, 147–184, 2010

DIAL measurement bias owing to surface reflectance variability

J. P. Lawrence et al.

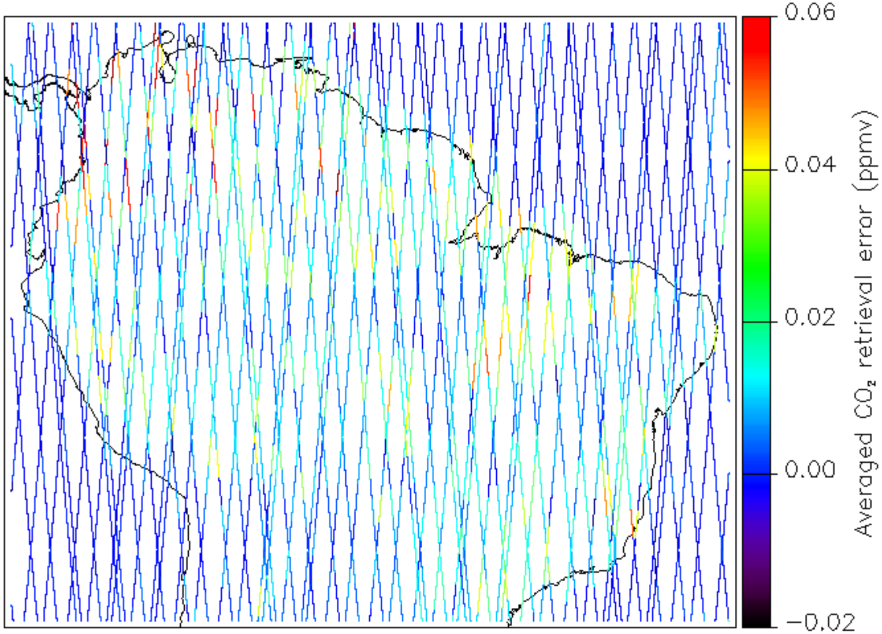

Fig. 9. CO_2 retrieval error in units of ppmv over South America for one month of 10 Hz simulated DIAL data integrated over 200 km intervals. The scale has been truncated to 0.06 to allow for stronger contrasts.

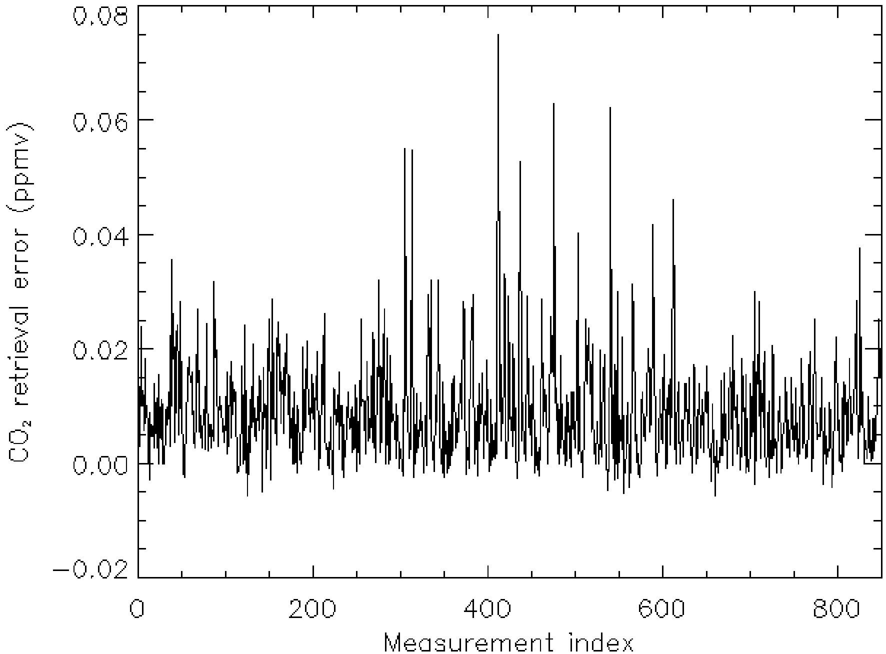

Fig. 10. CO_2 retrieval error in units of ppmv over Europe for one month of 10 Hz simulated DIAL data integrated over 200 km intervals.

AMTD
3, 147–184, 2010

DIAL measurement bias owing to surface reflectance variability

J. P. Lawrence et al.

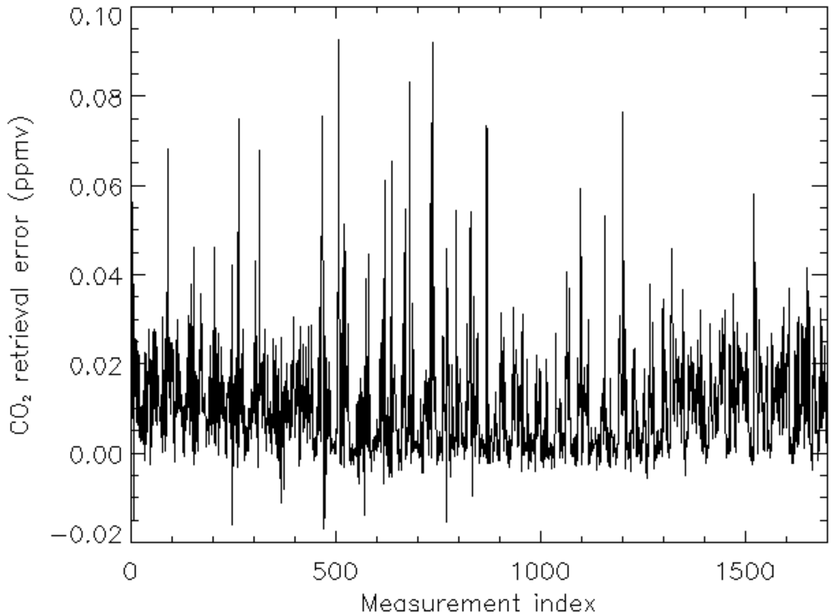

Fig. 11. CO_2 retrieval error in units of ppmv over South America for one month of 10 Hz simulated DIAL data integrated over 200 km intervals.

AMTD

3, 147–184, 2010

DIAL measurement bias owing to surface reflectance variability

J. P. Lawrence et al.

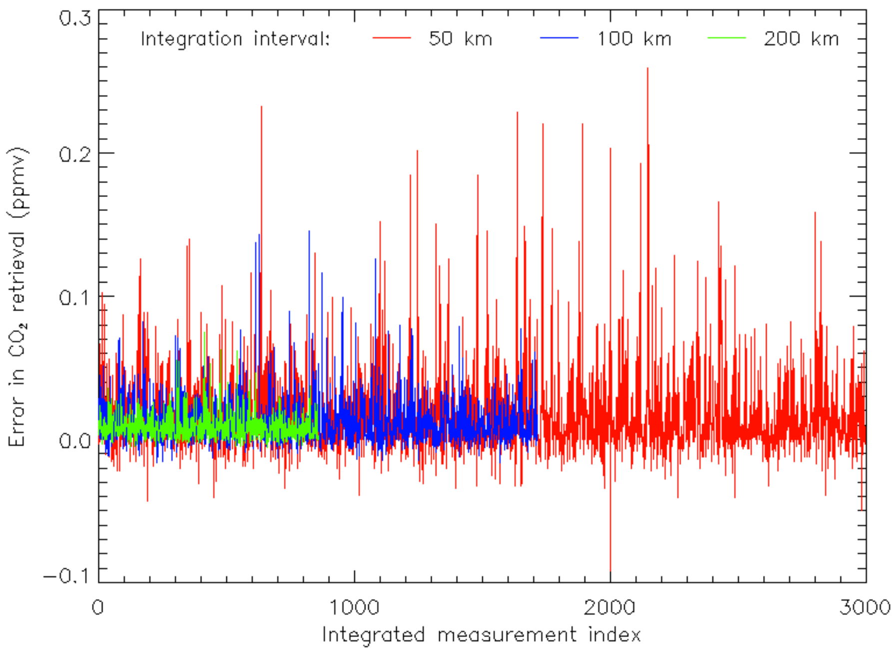

Fig. 12. CO_2 retrieval error in units of ppmv over Europe for 3 integration distance scenarios, 50 km, 100 km, and 200 km. A bias in retrieval error is seen to be present for all three integration distances.

AMTD

3, 147–184, 2010

AMTD

3, 147–184, 2010

DIAL measurement bias owing to surface reflectance variability

J. P. Lawrence et al.

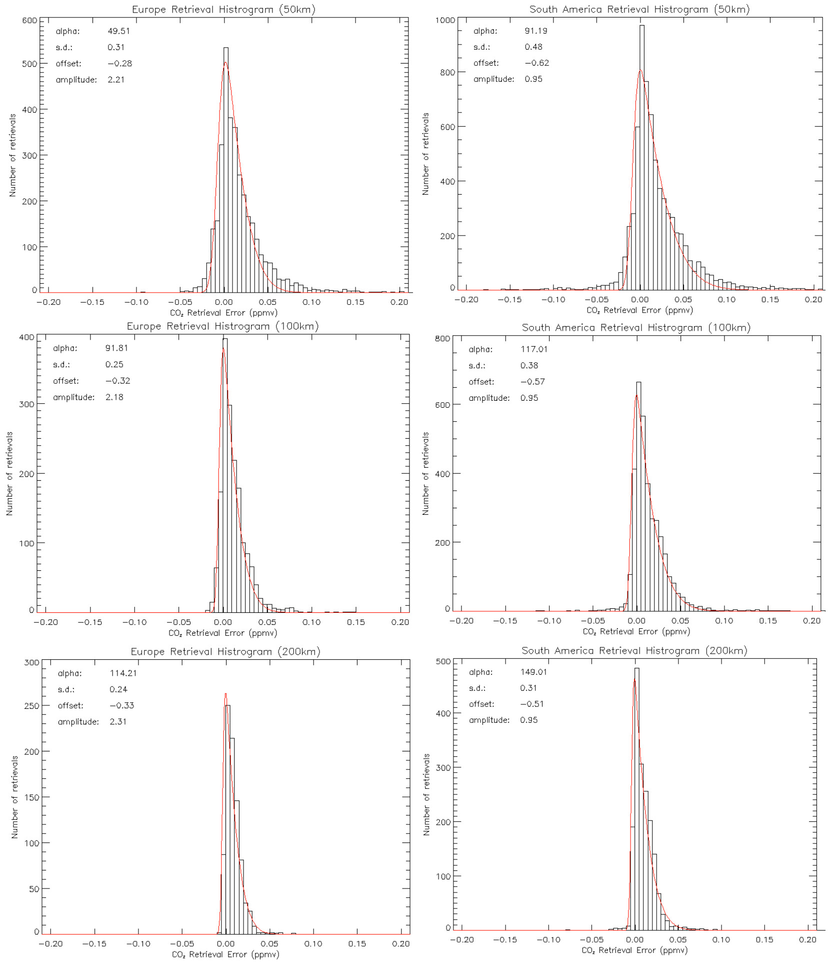

Fig. 13. CO_2 retrieval histrograms fitted with skewed normal distribution functions for the South America and Europe simulation results for 50, 100, and 200 km integration distances.

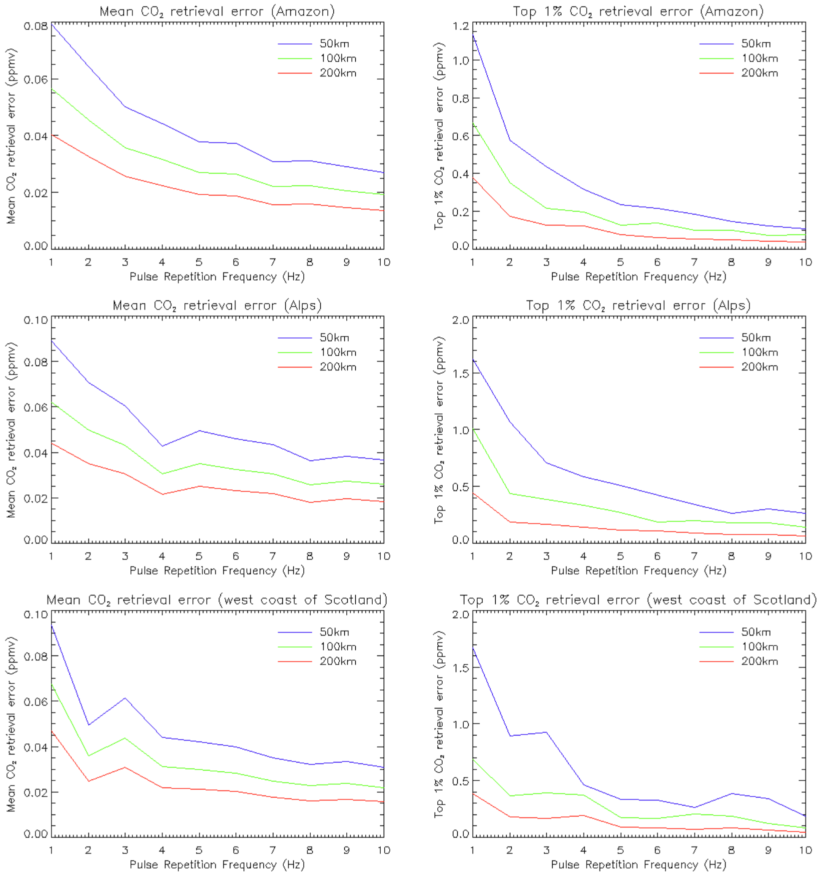

Fig. 14. CO_2 retrieval error over the Alps, the Amazon rainforest and the west coast of Scotland for 50, 100, and 200 km integration distances as a function of instrument pulse repetition frequency.

AMTD
3, 147–184, 2010

DIAL measurement bias owing to surface reflectance variability

J. P. Lawrence et al.